Journal Pre-proofs

Oxidative Dehydrogenation of Ethanol on Gold: Combination of Kinetic Experiments and Computation Approach to Unravel the Reaction Mechanism

Erfan Behravesh, Marko M. Melander, Johan Wärnå, Tapio Salmi, Karoliina Honkala, Dmitry Yu. Murzin

PII: S0021-9517(20)30296-7
DOI: https://doi.org/10.1016/j.jcat.2020.07.022
Reference: YJCAT 13834

To appear in: *Journal of Catalysis*

Received Date: 14 April 2020
Revised Date: 22 July 2020
Accepted Date: 24 July 2020

Please cite this article as: E. Behravesh, M.M. Melander, J. Wärnå, T. Salmi, K. Honkala, D. Yu. Murzin, Oxidative Dehydrogenation of Ethanol on Gold: Combination of Kinetic Experiments and Computation Approach to Unravel the Reaction Mechanism, *Journal of Catalysis* (2020), doi: https://doi.org/10.1016/j.jcat.2020.07.022

Oxidative Dehydrogenation of Ethanol on Gold: Combination of Kinetic Experiments and Computation Approach to Unravel the Reaction Mechanism

Erfan Behravesh[†], Marko M. Melander[‡], Johan Wärnå[†], Tapio Salmi[†], Karoliina Honkala[‡], Dmitry Yu. Murzin[†*]

[†] Johan Gadolin Process Chemistry Centre, Åbo Akademi University, FI-20500 Turku/Åbo, Finland

[‡] Department of Chemistry, Nanoscience Center, University of Jyväskylä, P.O. Box 35, FI-40014 Jyväskylä, Finland

Corresponding author: dmurzin@abo.fi

Abstract

Selective alcohol dehydrogenation on heterogeneous catalysts is a key industrial reaction for production of aldehydes, ketones, and carboxylic compounds. Design of catalysts with improved activity and selectivity requires understanding of the reaction mechanism and kinetics. Herein, experiments, density functional theory (DFT) and kinetic modelling were combined to elucidate the mechanism and kinetics of ethanol oxidative dehydrogenation to acetaldehyde on gold catalysts. Catalytic experiments clearly emphasized the role of oxygen in this reaction. Ethanol conversion was rather independent on the gold cluster size. Formation of minor products, acetic acid and ethyl acetate was structure sensitive as on smaller clusters ethanol is less prone to oxidation reacting more efficiently with acetic acid to ethyl acetate. DFT calculations indicated that the activation of molecular oxygen is facilitated by the hydrogen bond donor e.g., ethanol, leading to hydrogen abstraction from the bond donor and formation of an OOH intermediate followed by its facile dissociation. Furthermore, the calculations show that ethanol oxidation along such pathway is thermodynamically feasible on smooth Au(111) facets. The kinetic model developed based on the concept of ethanol mediated activation of oxygen derived from DFT studies, qualitatively and quantitatively by data fitting reproduces experimental observations on ethanol oxidative dehydrogenation over gold on alumina catalyst. The concentration profiles in the catalyst particle were calculated numerically to evaluate the role of diffusion in the catalyst pores. Combining experiments and DFT with kinetic modelling provides a powerful way to unravel the mechanisms and kinetics of heterogeneous catalytic reactions.

Keywords: ethanol oxidation, gold, mechanism, kinetics, DFT

1. Introduction

Selective oxidation of primary and secondary alcohols provides access to the corresponding aldehydes, ketones and carboxylic acids widely used in chemical industry [1–3]. Alcohols obtained from renewable resources, such as bioethanol, contribute to a decrease of dependency on fossil reserves [4]. Currently, ethanol is one of the most often applied biofuels. It is typically produced from biomass *via* fermentation and besides fuel applications it is used as a solvent in fuel cells, and as a feedstock for producing bulk chemicals via selective oxidation [5]. Considering the current and future surplus of bioethanol, importance of selective ethanol conversion to *e.g.* ethyl acetate and acetaldehyde is expected to increase [6].

Among various heterogeneous catalysts, oxide-supported gold-catalysts have attracted attention due to their stability and selectivity [7]. An important aspect of the oxidation catalysis by gold is the structure sensitivity. Conflicting results have been reported in the literature regarding the structure sensitivity in ethanol oxidative dehydrogenation, which can be related [8-11] to different supports, catalyst preparation methods, as well as reaction conditions (gas vs liquid phase, type of oxidant). Moreover, it is not always clear if other reactions occurring on acid supports (e.g. alumina) namely esterification and etherification reactions were subtracted from TOF calculations.

To understand and rationalize the observed discrepancies in structure- and size-dependent reactivity of supported gold-catalysts considerable experimental and computational research efforts have been put forward [13–26]. These studies highlight the importance of atomic-level understanding of the reaction mechanism and the nature of active sites on the catalyst surface to rationalize experimental results and to design better catalytic systems for Au-catalyzed alcohol oxidation. In mechanistic studies, it is important not to consider only the gold per se but also the support-metal interface which play a crucial role in the oxidation process, especially in the case of a reducible support such as titania [23–25]. However, for non-reducible supports

such as Al_2O_3 (the most frequently used support in industry) the impact of the support-metal interface is much less prominent to an extent that it is often neglected [26].

Previous experimental [27] and computational [28] studies have demonstrated that flat gold surfaces are unable to dissociatively adsorb O_2 because the dissociation barrier is very high (250 kJ/mol) and the desorption barrier is small (15-20 kJ/mol). Also the stepped Au(211) surface is unable the dissociate O_2 as the dissociation barrier (110 kJ/mol) is much higher than the desorption barrier (10 kJ/mol) [27] [28]. The same applies to the stepped and kinked Au(310) [29] where the dissociation barriers are smaller (60-110 kJ/mol) but still larger than the desorption barrier (0-25 kJ/mol). On the other hand, DFT computations suggest that some small, unsupported Au clusters can dissociate O_2 [30, 31] as the dissociation barrier is lower than the desorption barrier for some clusters. However, it is to be noted that most computational studies discussed above exclude the O_2 adsorption/desorption entropy and dispersion interactions. Accounting for dispersion effects will make adsorption more exothermic while entropic contributions will weaken O_2 binding by up to 50 kJ/mol [29]. For these reasons, calculations in [30, 31] do not provide a fully conclusive proof that small Au cluster can dissociate O_2. Indeed, if under-coordinated sites are responsible for the reported activity for alcohol oxidation, small nanoparticles should be more active than larger ones. Interestingly, the opposite behavior has been reported with larger gold particles (> ca. 7 nm), which were found to be more active than smaller ones [7].

Mechanistic aspects for alcohol oxidation have been studied both experimentally and theoretically [8, 13-23, 14, 32-38]. The reaction has been suggested to start with a metal-alkoxy formation followed by a β-hydride elimination, which generates a carbonylic product and a metal-hydride intermediate. DFT calculations have indicated that the presence of atomic oxygen enhances the cleavage of the ethanol O–H bond that is followed by β-H elimination [33]. Isotopic experiments for ethanol oxidation on O pre-covered Au(111) have revealed that

ethanol initially undergoes an O–H bond cleavage followed by the selective β–C–H bond activation of the corresponding ethoxide, which leads to the formation of acetaldehyde and water [39]. The catalytic activity of gold in oxidation reactions is typically attributed to the activation of molecular oxygen by the gold nanoparticles. The precise role of molecular oxygen in the alcohol oxidation has been explored by comparing oxidative dehydrogenation and dehydrogenation of ethanol on silica-supported gold catalysts [7]. From the kinetic viewpoint both reactions are of first order with respect to ethanol concentration, but the oxidative dehydrogenation is more rapid indicating that the presence of oxygen suppresses the activation energies of the key elementary steps [7]. Combined temperature programmed desorption and molecular beam reactive scattering studies have demonstrated that while the adsorption of methanol, propanol, and 2-butanol on a clean Au(111) surface is weak, all of them oxidize easily over an oxygen pre-covered Au(111) surface indicating that adsorbed atomic oxygen is necessary for the cleavage of a O-H bond [34, 35, 39].

Besides direct O_2 and O-H dissociation, both ethanol and molecular oxygen can be simultaneously activated by forming a hydrogen bond. Alternatively, O_2 may be activated using external hydrogen bond donors e.g., water, alcohols, and acids, which form a hydrogen bond interaction to O_2. This leads to hydrogen abstraction from the bond donor and the formation of an OOH (peroxide) intermediate followed by its facile dissociation [29, 40-44]. This mechanism might work even on highly coordinated Au sites producing reactive oxygen species and driving the alcohol oxidation towards carbonyl formation. Such a pathway, with the computed activation energy of 88 kJ/mol, has been proposed for methanol oxidation on Au(111) [40] with the reaction barrier is lower than for the direct O_2 dissociation pathway. However, the computed reaction energy is highly endothermic (120 kJ/mol) and therefore methanol oxidation is thermodynamically unfavorable. Yet, in these previous computational studies [29, 33, 40] on the hydrogen-bond assisted alcohol oxidation the O-H dissociation barrier is (when neglecting

adsorption entropy contributions) similar to the O_2 desorption barrier but accounting for adsorption entropy would likely make desorption more favorable than dissociation [29].

In the present work, catalytic experiments on ethanol dehydrogenation over gold on alumina in the presence and absence of oxygen in a wide temperature range, DFT calculations, and kinetic modelling were used to address ethanol oxidation behavior over Au catalysts. Experiments and DFT calculations suggest that ethanol oxidation follows a similar reaction mechanism as oxidation of methanol which is kinetically and thermodynamically feasible on Au(111) when van der Waals dispersion effects are taken into account in calculations. The DFT-proposed mechanism was then employed to develop a kinetic model and rate equations for ethanol oxidation. Finally, the calculations were compared with the experimental data, showing a good correspondence. Combining of experiments with DFT and kinetic modeling enables to conclusively unravel the mechanistic and kinetic details of ethanol dehydrogenation on alumina supported gold catalysts.

2. Experiments and methods

2.1. Catalyst preparation

The Au/Al_2O_3 catalysts were synthesized via deposition-precipitation using ammonia as the precipitating agent. Hydrogen tetrachloroaurate (ш) hydrate ($HAuCl_4.3H_2O$, 49 wt% Au) (Alfa Aesar and ABCR GmbH) was used as the gold precursor. The support was ɣ-Al_2O_3 (VGL-25) purchased from UOP Versal. First, alumina was dried at 100°C for several hours to evaporate the moisture inside the pores followed by immersing 4.7 g of ɣ-Al_2O_3 into 400 ml distilled water under vigorous stirring. The mixtures were stirred for 4 h and after that, some of the batches were heated up to 70°C at which to 170 ml 1.15 g/l gold solution the solution of ammonium hydroxide (32%, Merck) was added dropwise. Otherwise synthesis was done at 20°C. The mixture was stirred at 242 rpm for 3 h. For Au/Al_2O_3-1 catalyst synthesized at 70°C the pH raised from 8 to 8.5. Au/Al_2O_3-3 catalyst was also prepared at the same temperature

with pH elevation from 6.2 to 6.9. Other catalysts Au/Al_2O_3-2 and Au/Al_2O_3-4 were synthesized at room temperature at constant pH of 7.4 and 6.1 respectively. Afterwards, the catalysts were filtered, washed with 2 l of distilled water to remove chlorine species which was monitored by silver nitrate test. No turbidity in the washing solution was observed. The catalysts were dried over night at room temperature followed by drying at 80 (Au/Al_2O_3-3 and Au/Al_2O_3-4) or 100°C for 6-12 hours. Finally, the catalysts were calcined in a muffle oven at 300°C for 3 h.

2.2. Catalyst characterization

The catalysts were characterized by transmission electron microscopy (TEM), energy dispersive X-ray (EDX) and nitrogen physisorption. Electron microphotographs were obtained utilizing a JEM 1400 Plus transmission electron microscope with 120 kV acceleration voltage and resolution of 0.38 nm equipped with OSIS Quemesa 11 Mpix bottom mounted digital camera. The size distribution of the gold nanoparticles was obtained by counting about 100 particles. The metal dispersion was calculated from [45]:

$$D_{Au} = \frac{6M_{Au}}{a_{Au}\rho N_A d_{vs}} \quad (1)$$

where M_{Au} is the molar mass of gold (0.197 kg mol^{-1}), a_{Au} the average effective area of Au atom on the support surface (8.7 × 10^{-20} m^2), ρ the density of gold (1.932 × 10^4 kg m^{-3}), N_A the Avogadro number and d_{vs} is the volume–surface diameter calculated according to

$$d_{vs} = \frac{\sum d_i^3}{\sum d_i^2} \quad (2)$$

where d_i is the diameter of the gold cluster measured by TEM.

EDX (LEO Gemini 1530 with a Thermo Scientific UltraDry Silicon Drift Detector) was used to measure the gold content of the catalysts.

Sorptometer 1900 (Carlo Erba Instruments) was utilized to determine the specific surface area and the pore volume of the catalyst by nitrogen adsorption. Prior to the analysis, the catalyst was outgassed for 3 h at 150°C to remove the moisture and the air inside the alumina pores. The BET equation was used for the surface area calculations and the BJH method was applied to determine the volume of the mesopores.

2.3. Experimental setup and catalytic tests

The catalytic experiments were conducted under atmospheric pressure using 160 mg of the Au/Al_2O_3 catalysts with 20-32 μm average particle size in a quartz tubular fixed-bed reactor having the inner diameter of 9 mm. The inlet gas mixture contained ethanol, oxygen and helium (carrier gas). Liquid ethanol was fed by an HPLC pump (Shimadzu, LC-20AD) at room temperature and heated up to 100°C together with oxygen and helium to allow a gas phase mixture prior to the reactor. The total flow of the gas mixture at 100°C was 150 ml/min. The molar ratio of $EtOH/O_2/He$ was 1/3/10.2 at the reactor inlet. Ethanol dehydrogenation in absence of oxygen was performed with the same total flow having the inlet molar ratio of EtOH/He=1/13.2. Mass flow controllers Bronkhorst (HIGH-TECH) were used to adjust and control the oxygen and helium flows. In order to control the temperature inside the reactor, a PID controller (CalControls 9500 P) with a k-type thermocouple placed close to the catalyst bed (with ±1°C accuracy) was applied. The temperature inside the reactor was raised from 100°C stepwise by 25°C up to 250°C. The dwelling time at each temperature was 2.5 h and at least five samples were analyzed by GC to ensure that the differences in conversion as a function of time-on-stream are within analytical experimental errors and steady states are reached. At the reactor outlet the temperature was maintained at 130°C to prevent the condensation. The components were analyzed by an on-line gas chromatograph (Agilent Technologies, 7820A) equipped with both thermal conductivity (TC) and flame ionization (FI) detectors. The capillary column (HP-PLOT/Q) dimensions were 30 m length, 0.53 mm diameter

and 40 mm film of the immobile phase. The lines of the equipment were flushed with helium prior to each experiment.

2.4 Computational methods

Computational studies on the catalytic pathway were performed using the Density Functional Theory (DFT) code GPAW [46] which utilizes the projector-augmented wave method [47] to treat the core electrons. The Kohn-Sham equations were solved on a uniform real-space grid with a 0.18 Å grid spacing. The exchange-correlation effects were accounted for by using the BEEF-vdW –functional, which combines the generalized gradient approximation with the Langreth-Lundqvist van der Waals-functional [48] in an optimal way. The lattice constant of gold (4.24 Å) was optimized using 12x12x12 k-point sampling with a minimal unit cell. The surface calculations were performed for Au(111) using 3x3 non-orthogonal unit cell with five layers. The unit cell was periodic in x- and y-directions, the bottom two layers were fixed at the bulk positions while others were allowed to relax. 3x3x1 k-point sampling was utilized. The sufficiency of this 3x3x1 k-point sampling was checked by computing the adsorption energy of an EtOH-O_2 complex with a 4x4x1 k-point grid and the difference was found to be less than 2kJ/mol. More extensive k-point convergence tests in Ref [40] indicate that increasing the k-point mesh up to 7x7x1 has a only a moderate effect on adsorption energies and that 3x3x1 k-point sampling is accurate enough for the studied system with the errors due to a limited the k-point sampling being smaller than typical DFT errors. The Au(111) surface was selected to model the most stable and abundant facet of large Au nanoparticles. The support was neglected as the experimental studies did not exhibit size-effects beyond 2 nm particles, which indicates the support (interface) effects are not the determining factor. The structures were locally optimized with the FIRE optimizer [49] until the forces were below 0.05 eV/Å.

The transition states were located using the (climbing image) nudged elastic band (CI-NEB) [50, 51] method with 7-11 images as implemented in the Atomic Simulation Environment

(ASE) interface [52]. The initial guesses for the NEB calculations were obtained by performing a linear interpolation between the initial and final states. The linear initial pathway was pre-optimized using the image dependent pair potential (IDPP) [53]. The pathways were optimized using the FIRE optimizer [49] and considered converged when the total forces were below 0.1 eV/Å. For adsorption steps the entropic contributions were computed using the 3D and 2D rigid-rotor/translator approximations as implemented in ASE for gas-phase and adsorbed species, respectively, using 0.1 eV barriers.

3. Results and Discussion

3.1. Reaction scheme

Based on the analysis of literature data and our own experimental work and computations, the reaction mechanisms for the alcohol oxidation to aldehydes and ketones can be summarized as presented in Scheme 1. Ethanol and O_2 first adsorb on the catalyst surface, after which the reaction presumably proceeds via the direct O–H bond cleavage or *via* the atomic or molecular oxygen-assisted O–H bond breaking. This step is followed by the β–H elimination by an oxygen atom or a hydroxyl group leading to the formation of a carbonyl. The key step in the alcohol oxidation is the oxygen dissociation, which creates the reactive surface species.

(N^1)		(N^2)
2	$EtOH + * \rightarrow EtOH^*$	2
1	$O_2 + * \rightarrow O_2^*$	1
	Unassisted | Assisted	
1	$O_2^* + * \rightarrow 2O^*$	2
2	$EtOH^* + * \rightarrow EtO^* + H^*$	2
	$EtOH^* + O_2^* \rightarrow EtO^* + OOH^*$	
	$OOH^* + * \rightarrow O^* + OH^*$	
2	$O^* + EtO^* \rightarrow AcH * + OH^*$	2
0	$OH^* + OH^* \rightarrow H_2O^* + O^*$	2
2	$OH^* + H^* \rightarrow H_2O^* + *$	0
2	$AcH * \rightarrow AcH + *$	2
2	$H_2O^* \rightarrow H_2O + *$	2
0	$2O^* \rightarrow O_2^* + *$	1

Scheme 1. Reaction paths for EtOH dehydrogenation by O_2. $N^{(1)}$ with the corresponding stoichiometric numbers reflects the route where ethanol is adsorbed with dissociation, while $N^{(2)}$ describes the route where OH breaking in ethanol is assisted with oxygen.

3.2. DFT analysis of ethanol oxidation on Au(111)

3.2.1 Adsorption of reactants and reaction intermediates

To gain mechanistic insight for ethanol oxidation on Au(111), adsorption of reactants and intermediates was considered first. Figure 1 shows the most stable adsorption geometries for these species.

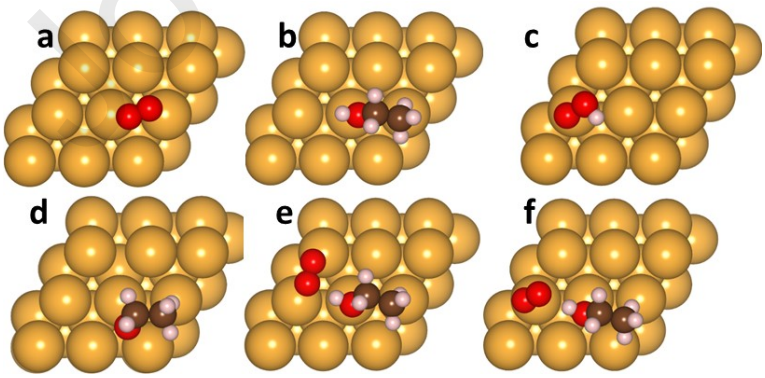

Figure 1 The most stable adsorption geometries of a) O_2, b) EtOH, c) OOH, d) EtOH, e) EtOH-O_2 (bridge), and f) EtOH-O_2(top).

The adsorption and activation of molecular oxygen on Au(111) has been extensively studied experimentally and computationally in literature [20, 32, 54] . In agreement with previous calculations, it was found in the current work that O_2 adsorbs in a parallel orientation over top and bridge sites with the mildly exothermic adsorption energy of -31 kJ/mol. As the accuracy of the used BEEF-vdW functional is ± 25 kJ/mol for weakly bound systems [55], O_2 adsorption is nearly thermoneutral or slightly endothermic. Including entropy effects makes the adsorption at room temperature almost thermoneutral as the free energy change is only -4 kJ/mol. Upon adsorption, O_2 retains its gas-phase triplet state and the bond length (1.23 Å), meaning that the molecule is not activated and thus the adsorption can be considered as physisorption. Previous computational studies [40, 56, 57] predict endothermic O_2 adsorption energies on Au (111) but these studies excluded van der Waals contributions.

We find that ethanol adsorbs *via* the O atom of the OH-group on a top position at Au(111). DFT calculations give two distinct adsorption configurations (Figure 1b) which differ from each other by the Au-O bond length. Adsorption energies are mildly exothermic -19 kJ/mol and -28 kJ/mol for both geometries and the corresponding Au-O distances are 3.40Å and 2.85 Å, respectively. Including entropy effects at standard conditions makes EtOH adsorption slightly endothermic by 10 kJ/mol. The energetically more favorable adsorption configuration agrees well with recent computational results [58] which explore the influence of vdW interactions on ethanol adsorption characteristics. Depending on the flavor of the employed vdW functional, the computed adsorption energies vary between -20 and -50 kJ/mol while the Au-O bond length changes in the range of 2.6-2.8 Å [58]. Ethanol adsorption energy on Au(111) is only -9 kJ/mol if the vdW contribution is neglected [33].

For co-adsorption of EtOH and O_2, adsorption energy is -63 kJ/mol, which is 5 kJ/mol more exothermic compared to the sum of adsorption energies of individually adsorbed EtOH and O_2

species. Further stabilization of the EtOH-O_2 complex is achieved when O_2 transfers from the bridge position to a top site next to ethanol. In that case, the co-adsorption energy is -69 kJ/mol, which is -11 kJ/mol more exothermic than having reactants adsorbed separately. Accounting for entropy contributions makes the co-adsorption thermoneutral at normal conditions. For both adsorption complexes, the stabilization effect can be attributed to the formation of a hydrogen bond (OH-O_2 length is 1.91 Å) between molecular oxygen and ethanol. The vicinity of the molecule introduces changes to the adsorption characteristics of the other molecule in a way that O_2 prefers a singlet electronic state, with the O-O bond length of slightly elongated to 1.29Å. Simultaneously, the presence of O_2 makes EtOH to bind closer to the surface decreasing the Au-O distance to 2.75 Å. Altogether these changes suggest that the Au-complex interaction resembles chemisorption rather than physisorption. Interestingly, clearly exothermic adsorption of the EtOH-O_2 complex Au(111) differs significantly from that of methanol and O_2, which was found endothermic by 42 kJ/mol according to DFT [46]. Presumably, the main reason for this difference is the exclusion of vdW interactions from the methanol oxidation study [40].

Along the reaction pathway from O_2 and EtOH to H_2O and acetaldehyde (AcH), the main intermediates are hydroperoxyl (OOH), O and OH formed from OOH, and ethoxy (EtO) formed after hydrogen cleavage from the OH group of EtOH. The most stable adsorption geometry for OOH is shown in Figure 1 d. In the second-best geometry, hydroperoxyl binds through both oxygens to two Au atoms and this configuration is 13 kJ/mol higher in energy. Both of these geometries have been considered for reaction pathways, described in the next section. The OOH dissociation products, an O-atom and OH group, adsorb on three-fold and bridge sites, respectively. The ethoxy intermediate binds to Au(111) *via* the oxygen atom on a bridge site, (Figure 1 c) and acetaldehyde does not stay in contact with Au(111) but desorbs spontaneously.

3.2.2 Direct and oxidative dehydrogenation of ethanol

Direct dehydrogenation of ethanol to ethoxy will be considered prior to oxidative dehydrogenation of ethanol. Following previous computational studies for methanol and ethanol oxidation on Au(111) [33, 45] and experimental studies on ethanol oxidation on Au(111) [37], the first elementary step is assumed to be the cleavage of the O-H bond followed by the C-H bond breaking. It was found that after an O-H bond cleavage ethoxy and H bind to bridge and hollow sites, respectively. The activation barrier is computed to be very high being 215 kJ/mol with respect to adsorbed ethanol and the reaction energy is 149 kJ/mol making this elementary step kinetically and thermodynamically implausible. These results are in line with computational findings for methanol [40] and ethanol dehydrogenation on Au(111) [33]. In previous calculations, the second dehydrogenation step was found kinetically even less favorable than the first one and therefore it was omitted from considerations.

The activation of O_2 and the role of oxygen in alcohol oxidation on Au are still heavily debated in the literature. Experimental studies on supported Au catalysts [30] demonstrated activity for ethanol dehydrogenation in the absence of oxygen but in the presence of oxygen activity substantially increases, whereas surface science experiments on Au single crystal surfaces [59] show no dehydrogenation reactivity without atomic oxygen. Introducing atomic oxygen on Au(111), makes the surface highly active for alcohol oxidation, which is seen both in experiments [32, 36, 39] and calculations [29, 33, 41] . However, no final conclusions have been reached whether atomic oxygen generated in O_2 dissociation or molecular oxygen is the reactive species.

The computed reaction energy for O_2 dissociation from the bridge geometry to two oxygen atoms on adjacent hollow sites is 31 kJ/mol. At the transition state, the O-O bond length is substantially elongated compared to gas-phase molecule being 1.88Å and the corresponding activation energy is 173 kJ/mol. This indicates that dissociative adsorption of O_2 on Au(111) is highly unlikely even though here a somewhat lower barrier is reported than previous literature

values of 235 kJ/mol [45] and 215 kJ/mol [60]. Again, the activation energy difference can be attributed to inclusion of the van der Waals interactions into the present study. The DFT results clearly show that unassisted O_2 dissociation and O-H bond cleavage from ethanol are unfeasible on Au(111) and therefore alternative mechanistic pathways are considered.

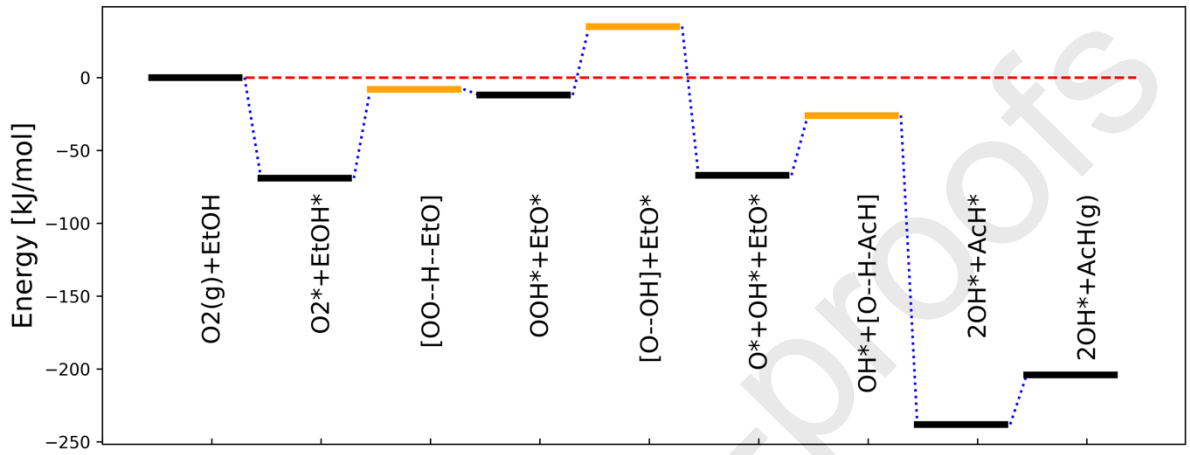

Figure 2. The minimum energy path for the assisted EtOH dehydrogenation. The black and orange bars correspond to minima and transition states, respectively. * denotes adsorbed species, while (g) refers to gas phase species. Square brackets enclose a transition state structure where ' - -' marks the bond being broken.

Figures 2 and 3 present a potential energy surface and mechanistic details of an O_2 assisted ethanol oxidation pathway, respectively. The initially formed O_2-EtOH complex reacts to form OOH and EtO *via* breaking the O-H bond with the help of O_2. The transition state strongly resembles the OOH intermediate, and thus the activation energy, 61 kJ/mol, is close to the thermodynamic barrier, which is 57 kJ/mol. Accounting for vibrational contributions slightly increases the barrier (75 kJ/mol) which is again close to the thermodynamic barrier of 71 kJ/mol. Because the activation energy is higher than desorption energy for O_2 and ethanol, the desorption is more favorable than O-H bond cleavage.

Once OOH has been formed, it can break down rather easily to atomic oxygen and a hydroxyl group. Starting from the higher-energy hydroperoxyl (bound from two oxygens to two Au

atoms), its transfer to the more stable top-site bound hydroperoxyl and therefore pathways from this site are reported herein. In the presence of EtO, the OOH decomposition has a barrier of 47 kJ/mol and the reaction is exothermic by -55 kJ/mol. On the bare Au(111) surface, the barrier is 64 kJ/mol and the reaction energy is -61 kJ/mol. This indicates that the presence of EtO helps the cleavage of the O-O bond probably by providing an additional H-bonding. Once the reactive oxygen species (O-H and O) have been formed, they can easily dissociate the O-H bond as shown in [40] to form water or hydroxyl groups.

The next step is the β–H elimination, which can be assisted by an O atom, a OH group or possibly OOH species. As the dissociation of OOH proves to be facile, the most reactive species, namely an O atom has been investigated. The atomic oxygen readily breaks the C-H bond forming acetaldehyde. The barrier for C-H cleavage is 41 kJ/mol and the reaction is highly exothermic by -212 kJ/mol. In the present work, desorption energy of adsorbed AcH is 34 kJ/mol. The activation energy is 22 kJ/mol higher than the previously computed value for β-H elimination of ethoxy but that, again, was obtained without vdW interactions and it is substantially lower than the barrier computed on bare Au(111), which has reported to give the activation barrier over 250 kJ/mol [33]. Barrier heights and reaction energetics for formaldehyde formation are similar to our values if β–H was cleaved with the help of O, OH or OOH species [45]. In H_2O formation, OOH-derived hydroxyl is the key intermediate and is obtained when OH combines with hydrogen produced by cleaving either an O-H or a C-H bond. Both of these bond-breaking steps are reported to have low barriers E_{act} ~ 10 kJ/mol and E_{act} ~ 24 kJ/mol [40] for O-H and C-H, respectively. A single water molecule binds weakly on Au(111) (E_{ads}=-33 kJ/mol) and can desorb readily. The product molecules water and AcH are highly stable in gas-phase providing the thermodynamic driving force of the entire reaction scheme. The formation of AcH and water (not shown in Figure 3) was also experimentally observed as discussed in Section 3.3.

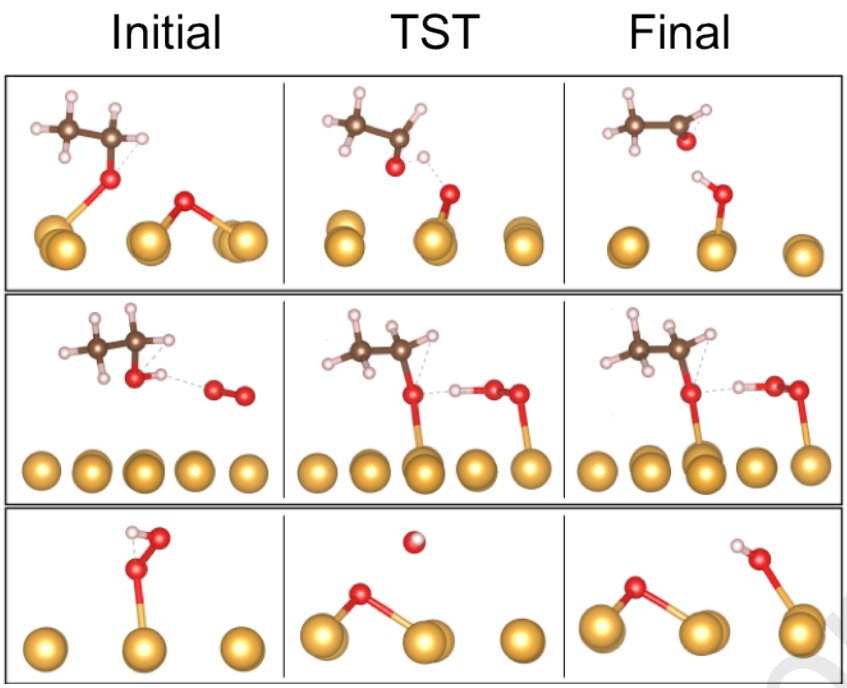

Figure 3. From top-to-bottom: β-H elimination forming acetaldehyde, O_2 assisted O-H dissociation, and OOH dissociations. The left (right) image depicts the initial (final) state while the central image is the transition state. The dashed line indicates hydrogen bonding. The color scheme is as follows: Au atoms are yellow, C atoms brown, O atoms red, and H atoms white.

In line with the previous calculations for methanol [40] and ethanol [33], calculations in this work suggest that ethanol dehydrogenation is facilitated by synergetic effects between O_2 and EtOH and van der Waals dispersion effects. The adsorption of O_2 and EtOH is very weak and the desorption is more favorable than the step O_2→OOH which has the highest barrier for the overall reaction. However, once OOH dissociates to O and OH, the formation of AcH proceeds with a small barrier and high thermodynamic driving force which makes the reaction proceed towards the products. Once the reaction is initiated, the oxygen [32, 61] and hydroxyl [33] species can provide even a more reactive environment for the EtOH dehydrogenation. Further enhancement of EtOH dehydrogenation is facilitated by the presence of additional hydrogen bond donors and acceptors such as H_2O, acids, silanes, amines *etc*. [39], which can assist the dissociation of both the O-O and O-H bonds. Moreover, small particles and uncoordinated sites are known to be more effective in the dissociation of the O-O bond providing an additional possibility to enhance the activity [28].

3.3. Catalytic ethanol oxidation

3.3.1. Catalyst characterization

The catalyst characterization results are summarized in Table 1 with the gold particle size distribution presented in Figure 4. As can be seen the metal loading was close to 1 wt% and the average particle size was ranging between ca. 2 and 7 nm. Figure 4 illustrates that the catalysts with a smaller average gold nanoparticle size have also narrower particle size distributions

Table 1. Characterization results of the Au/Al_2O_3 catalysts

Catalyst entry	Au average particle size (nm)	Au dispersion (%)	Au loading (wt%)	Catalyst specific surface area (m^2g^{-1})	Catalyst pore specific surface area (m^3g^{-1})
1	1.9	41.6	0.77	274	0.89
2	3.6	25.7	0.76	—	—
3	5.1	16.8	1.36	341	1.11
4	6.9	13	1.7	—	—

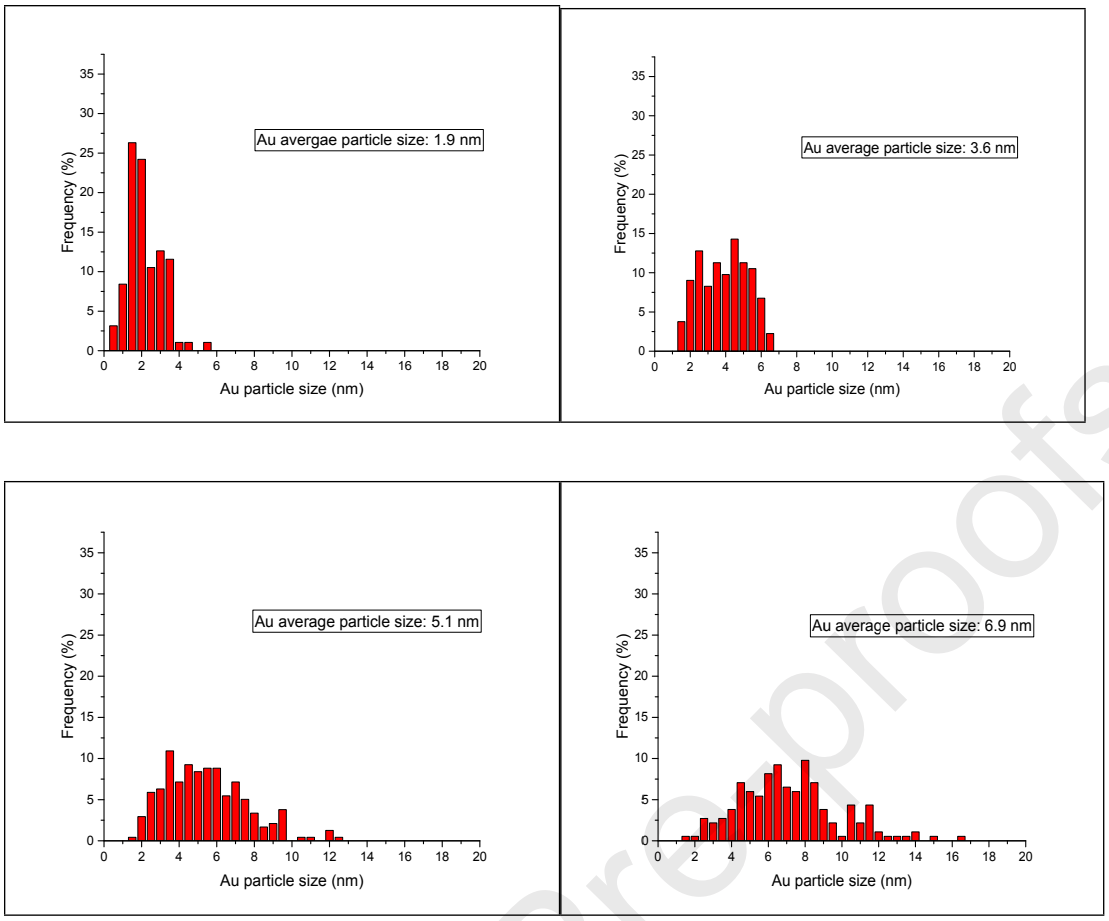

Figure 4. Particle size distribution of the Au/Al_2O_3 catalysts

3.3.2. Ethanol dehydrogenation in absence of oxygen

To reveal the role of oxygen, the catalysts were exposed to ethanol in the absence of oxygen within the temperature range between 100-250°C. It should be noted that temperature hysteresis behavior in these and other experiments was negligible, i.e. no meaningful differences in conversion were observed, when the same temperature point was reached by either decreasing or increasing temperature. Similar results have been reported previously by the authors for oxidation of ethanol in a microreactor [62].

Figure 5 demonstrates that the conversion of ethanol in the absence oxygen increased up to 52% at the highest considered temperature. At 125°C acetaldehyde is the sole product but the ethanol conversion was only 0.08 %. At higher temperatures the selectivity diminished significantly being only 5 % at 250°C. Diethyl ether is the main product at temperatures above 150°C.

Ethanol dehydration to ethylene was observed from 200°C upwards increasing slightly up to 6 % at the highest temperature used in experiments. Small differences in conversion for different catalysts can be attributed to the differences in metal dispersion and surface areas of the catalysts.

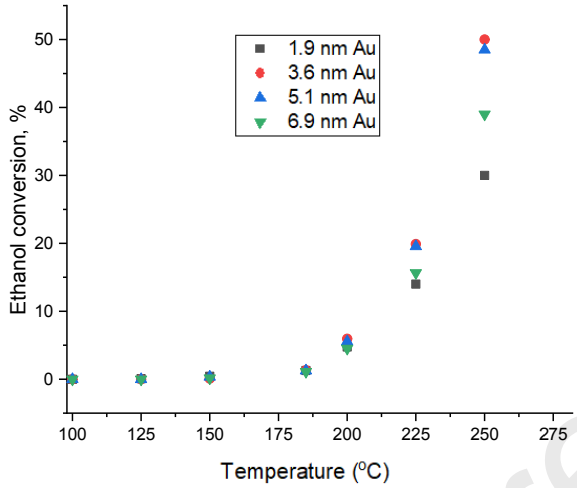

a)

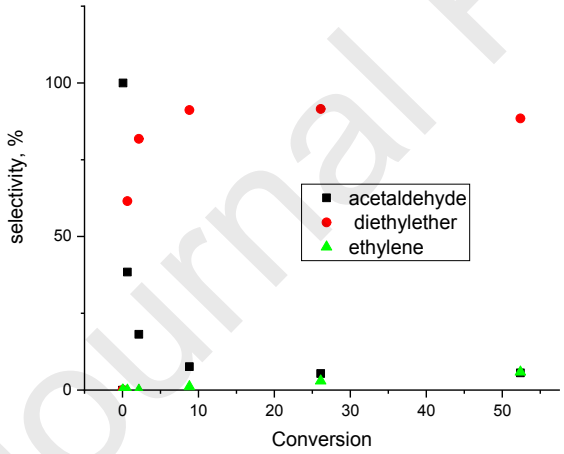

b)

Figure 5. Ethanol dehydrogenation in the absence of oxygen: a) conversion for all catalysts and b) selectivity dependence on conversion for the catalyst with 1.9 nm Au cluster size.

3.3.3. Ethanol dehydrogenation in presence of oxygen

The dehydrogenation of ethanol in the presence of oxygen was conducted to explore the influence of oxygen on the product selectivity. The reaction was conducted in the temperature

range of 100-250°C. Figure 6 illustrates that the conversion of ethanol in presence of oxygen was higher compared to the values obtained in the absence of oxygen (Figure 5) up to 225°C whereas after 250°C the conversion of ethanol was the same both in the presence and absence of oxygen (52 %).

The results in Figure 6a show that the ethanol conversion is rather independent on particle size. However, the product distribution and selectivity depend on the particles size as shown in Figure 6. The main product with the highest selectivity over the studied catalysts was acetaldehyde (Figure 7). The minor product selectivity depends on the particles size and unlike dehydrogenation of ethanol in the absence of oxygen, acetic acid and ethyl acetate were formed. The main by-product for the smallest particles is ethyl acetate whereas for the larger particles there is predominant formation of diethyl ether by dehydration on acid sites. For the former case the ethyl acetate selectivity increased up to 30 % at the highest temperature. Ethylene and CO_2 were not detected for this catalyst. Significantly lower amounts of diethyl ether were observed giving 4.5 % selectivity at 250°C for the catalyst with lowest gold cluster size. These values increased as the gold particle size increased (Figure 7). A tentative explanation for the structure sensitive selectivity could be that on the catalyst with small particle sizes ethanol reacts preferentially with acetaldehyde, which is stronger adsorbed on such clusters, at the expense of etherification reaction than with another molecule of ethanol on the acid sites.

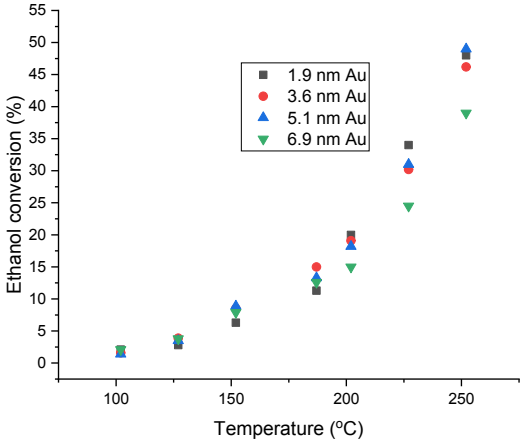

a)

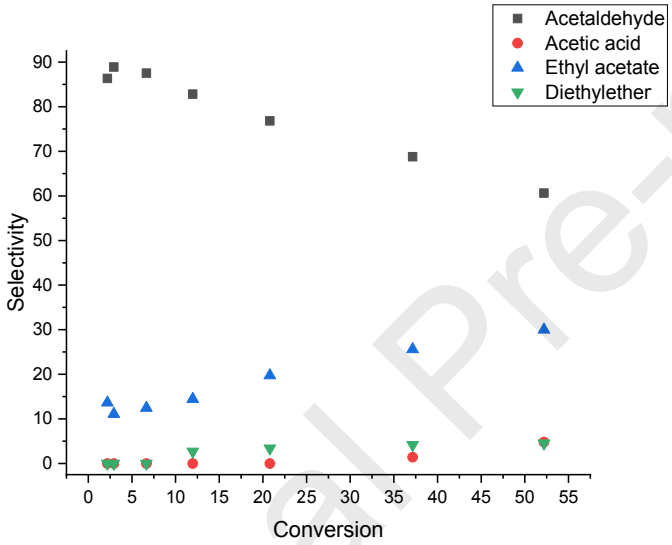

b)

Figure 6. Ethanol dehydrogenation in the presence of oxygen [61] a) conversion over different catalysts and b) selectivity over the catalyst with 1.9 nm Au cluster size.

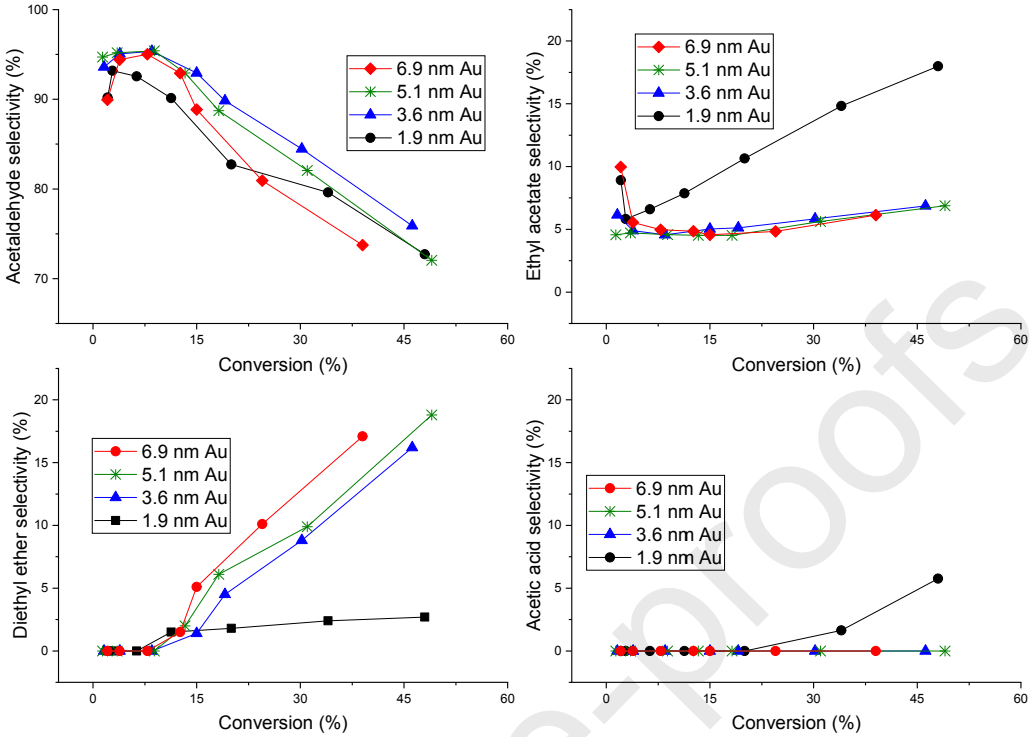

Figure 7. Selectivity of the main products of ethanol dehydrogenation reaction in the presence of oxygen at different conversions

3.3.4. Kinetic modelling of ethanol oxidation on gold catalyst

To further elucidate the mechanism and kinetics associated with ethanol oxidation on the gold catalyst, a kinetic model was developed to explain the measured reaction rates towards the desired product, acetaldehyde. The mechanism behind the kinetic model was inspired by the computational studies and can be presented as follows:

	$N^{(2a)}$	$N^{(2b)}$	$N^{(2c)}$	
1. $O_2+*\Xi O_2*$	1	1	1	
2. $EtOH+*\Xi EtOH*$	2	2	1	
3. $EtOH* + O_2*\leftrightarrow EtO*+OOH*$	2	1	2	(3)
4. $OOH*+*\rightarrow O*+OH*$	2	1	1	
5. $O*+EtO*\rightarrow AcH+*+OH*$	2	2	2	
6. $2OH*\leftrightarrow O*+H_2O+*$	2	2	2	
7a. $2O*\rightarrow O_2*+*$	1	0	0	
7b. $EtOH*+O*\rightarrow EtO*+OH*$	0	1	0	
7c. $O*+OOH*\rightarrow O_2*+OH*$	0	0	1	
$N^{(2)}$ $2EtOH+O_2\rightarrow 2AcH+2H_2O$				

According to the DFT calculations the mechanism $N^{(1)}$ in Figure 1 was considered to be unfeasible, therefore kinetic analysis was performed only for the mechanism $N^{(2)}$. The activation barrier for step 7a, i.e. recombination of atomic oxygen, is anticipated to be rather high, thus other options in principle can be considered (steps 7b and 7c). In the derivation below and eventual kinetic modelling the mechanism $N^{(2b)}$ was implemented representing a feasible channel of atomically adsorbed oxygen consumption with a low activation energy barrier of ca. 20 kJ/mol [32].

On the right hand side of the equations for the steps the stoichiometric numbers along the routes $N^{(2a)}$ - $N^{(2c)}$ are given [63]. These numbers can be equal to zero, if a particular step is not involved in the reaction mechanism. Steps 1 and 2 are considered to be at quasi-equilibria. Because of the substantial differences in activation energy for the forward and reverse reactions, the steps 4 and 5 were considered are irreversible, while the steps 3 and 6 are reversible. In eq. (3) EtOH stands for ethanol, while AcH represent acetaldehyde and *denotes a surface site. The coverages of surface species involved in quasi-equilibria steps can be easily written

$$\theta_{EtOH} = K_2 C_{EtOH} \theta_V ;\ \theta_{O_2} = K_1 C_{O_2} \theta_V \qquad (4)$$

where θ_{EtOH} and θ_{O_2} correspond to the coverages of ethanol and dioxygen, while θ_V denotes the fraction of vacant sites. C_{EtOH} and C_{O_2} denote the ethanol and oxygen concentrations, respectively, and where k and K are the rate and equilibrium constants for respective steps. From the steady state approximation for steps 5 and 7b

$$r_5 = 2r_{7b} \qquad (5)$$

One gets

$$\theta_{EtO} = \frac{2k_{7b}K_2 C_{EtOH}}{k_5}\theta_V \qquad (6)$$

Other steady state conditions

$$r_3 = r_{7b};\ 2r_4 = r_6;\ r_3 = r_4$$

give respectively expressions for coverage of other species

$$\theta_O = \frac{k_3 k_4 K_1 C_{O_2}}{k_{7b}(k_4 + k_{-3}\frac{k_{7b}}{k_5} C_{EtOH})} \theta_V \quad (7)$$

$$\theta_{OH} = \theta_V \sqrt{\frac{2}{k_6}\left(\frac{k_3 k_4 K_1 K_2 C_{O_2} C_{EtOH}}{k_4 + k_{-3}\frac{k_{7b}}{k_5} C_{EtOH}} + \frac{k_{-6} k_3 k_4 K_1 C_{O_2} C_{H_2O}}{k_{7b}(k_4 + k_{-3}\frac{k_{7b}}{k_5} C_{EtOH})}\right)} \quad (8)$$

$$\theta_{OOH} = \frac{k_3 K_1 K_2 C_{O_2} C_{EtOH}}{k_4 + k_{-3}\frac{k_{7b}}{k_5} C_{EtOH}} \theta_V \quad (9)$$

The conservation equation for the coverage is

$$\sum \theta = \theta_V + \theta_{EtOH} + \theta_{O_2} + \theta_O + \theta_{EtO} + \theta_{OOH} + \theta_{OH} \quad (10)$$

Giving

$$\theta_V = \frac{1}{1 + K_2 C_{EtOH} + K_1 C_{O_2} + \frac{2k_{7b} K_2 C_{EtOH}}{k_5} + \frac{k_3 k_4 K_1 C_{O_2}}{k_{7b}(k_4 + k_{-3}\frac{k_{7b}}{k_5} C_{EtOH})} + \sqrt{\frac{2}{k_6}\left(\frac{k_3 k_4 K_1 K_2 C_{O_2} C_{EtOH}}{k_4 + k_{-3}\frac{k_{7b}}{k_5} C_{EtOH}} + \frac{k_{-6} k_3 k_4 K_1 C_{O_2} C_{H_2O}}{k_{7b}(k_4 + k_{-3}\frac{k_{7b}}{k_5} C_{EtOH})}\right)} + \frac{k_3 K_1 K_2 C_{O_2} C_{EtOH}}{k_4 + k_{-3}\frac{k_{7b}}{k_5} C_{EtOH}}} = \frac{1}{D} \quad (11)$$

The overall rate of the reaction is equal to the rate of any step in the catalytic cycle, thus the final expression for the reaction rate of acetaldehyde formation $r^{(acetaldehyde)}$ is

$$r^{(acetaldehyde)} = r^{(N^{2b})} = k_4 \theta_{OOH} \theta_V = \frac{k_3 k_4 K_1 K_2 C_{O_2} C_{EtOH}}{(k_4 + k_{-3}\frac{k_{7b}}{k_5} C_{EtOH}) D^2} \quad (12)$$

where $r^{(N^{2b})}$ stands for the overall reaction rate along the route N(2b) and D is the denominator in eq. (11).

The estimation of the kinetic parameters was performed for the experimental data generated for catalyst 1 as an example using the ModEst parameter estimation software [64]. Preliminary calculations allowed some simplification of eq. (12) resulting in the simplified rate equation

$$r^{(acetaldehyde)} = r^{(N^{2b})} = \frac{k_I C_{O_2} C_{EtOH}}{(1 + K_2 C_{EtOH} + K_1 C_{O_2})^2} \quad (13)$$

where k_I is a lumped constant $k_I = k_3 K_1 K_2$.

To account for the side products (ethyl acetate and diethyl ether) formation, the following reactions were considered

$$EtOH + AcH + 0.5O_2 \rightarrow EtAc + H_2O \quad (14)$$

$$2EtOH \rightarrow DEE + H_2O \quad (15)$$

where EtOH, AcH, EtAc and DEE are ethanol, acetaldehyde, ethyl acetate and diethyl ether, respectively. Formation of ethylene was neglected because it was obtained in trace amounts only. The following kinetic equations were considered in addition to eq. (13), diethyl ether

$$r^{(ethyl\_acetate)} = k_{II} C_{O_2} C_{EtOH} C_{AcH} \quad (16)$$

$$r^{(diethyl\_ether)} = k_{III} C^2_{EtOH} \quad (17)$$

The mass balances of the components are listed below assuming that there are no diffusion limitations and that the plug flow prevails.

$$\frac{d\dot{n}_{EtOH}}{dz} = m_{cat}(-r^I - r^{II} - 2r^{III}) \quad (18)$$

$$\frac{d\dot{n}_{Ac}}{dz} = m_{cat}(r^I - r^{II}) \quad (19)$$

$$\frac{d\dot{n}_{EtAc}}{dz} = m_{cat} r^{II} \quad (20)$$

$$\frac{d\dot{n}_{DEE}}{dz} = m_{cat} r^{III} \quad (21)$$

where m_{cat} is the catalyst mass, $\dot{n}$ is the molar flow and z is the relative reactor length (z $\in$[0,1]). The rate constants were presumed to obey the Arrhenius law. The modified Arrhenius

equation [65] was used to suppress the correlation between the pre-exponential factor and the activation energy,

$$k_i = k_{i,mean} \exp\left[\frac{-E_{act}}{R}\left(\frac{1}{T}-\frac{1}{T_{mean}}\right)\right] \quad (22)$$

where k_i, $k_{i,mean}$, E_{act}, R, T and T_{mean} denote the reaction rate constant, the reaction rate constant at the mean temperature (175°C), activation energy of the reaction, the universal gas constant, the temperature and the mean temperature, respectively.

The objective function *(Q*) was set to minimize the degree of explanation between the calculated and experimental values of concentrations

$$\bar{n}_{est}\ Q = \max R^2 = \max 100\left(\frac{(\|n_{\exp} - n_{est}\|)^2}{(\|n_{\exp} - \bar{n}_{est}\|)^2}\right) \quad (23)$$

The degree of explanation, defined as the ratio of the squared difference in the experimental (n_{exp}) and the estimated (n_{est}) values of molar fluxes of all components, and the square of the differences between n_{exp} and the mean of the estimated molar fluxes $\bar{n}_{est}$, reflects a comparison between the residuals given by the actual model with the residuals of the simplest model, *i.e.* the average value of all data points [65]. The parameter estimation was done for the whole data set at all temperatures (100-250^{o}C) and initial concentrations simultaneously by numerically solving the differential equation (12) with the Levenberg-Marquart method incorporated in the software.

The value of the activation energy for the step 3 derived from DFT calculations, i.e. 75 kJ/mol was used directly in numerical data fitting.

Preliminary calculations indicated that the estimated values of the equilibrium constants are not reliable and therefore the statistical analysis was conducted using the Monte Carlo Markov Chain (MCMC) method [66]. In this method the samples are drawn randomly to approximate

the probability distribution of parameters. The MCMC method, incorporated in the optimization software ModEst, provides a tool for the evaluation of the reliability of the model parameters by treating all the uncertainties in the data and the modelling as statistical distributions [67]. The results of statistical analysis are illustrated in Figure 8, showing the most probable values of constants as maxima [68].

Based on statistical analysis (Figure 8) the values of constants were fixed at K_1=0.00082 m^3/mol, K_2=0.0054 m^3/mol during parameter estimation, while the values of activation energies were fixed at E_{actII}=15 kJ/mol and E_{actIII}=105 kJ/mol as follows from Figure 8.

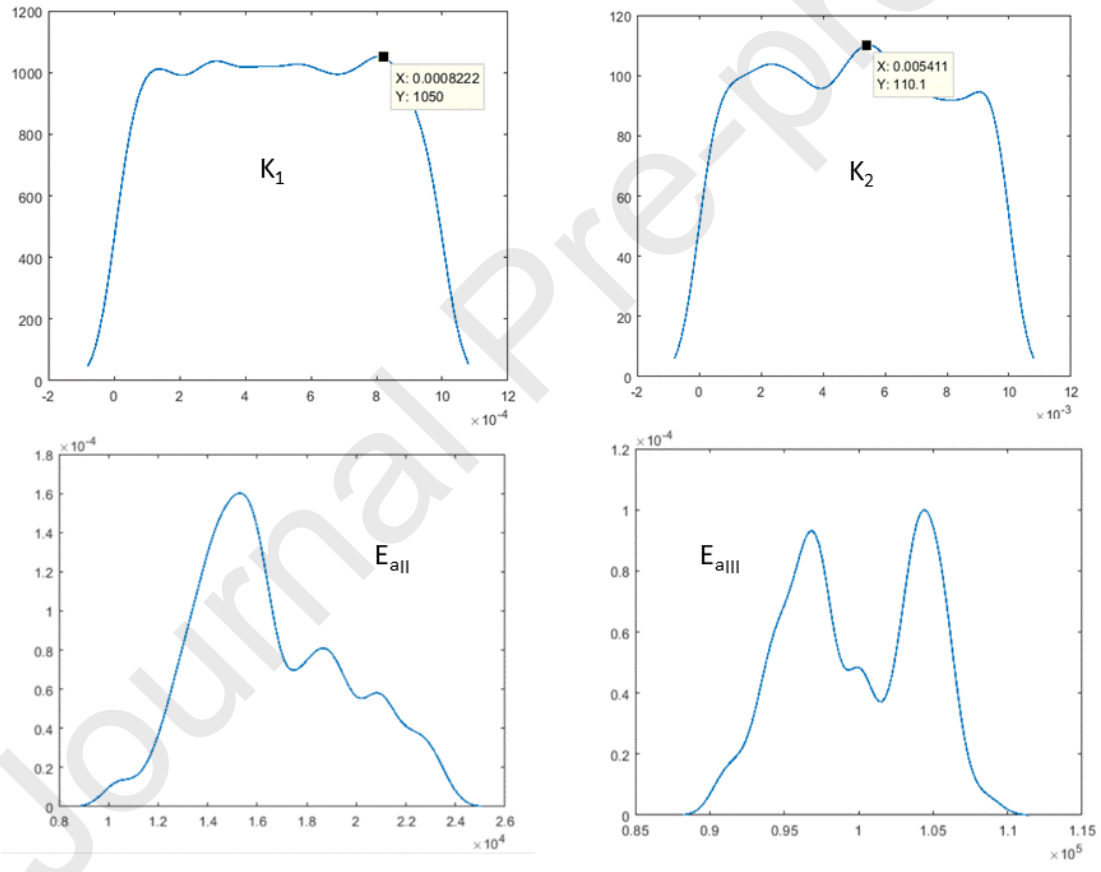

Figure 8. Statistical analysis of the adsorption constants by MCMC method showing posterior distributions for the parameters (y-axes) reflecting their probability vs parameter values (x-axes) . The most probable values of parameters are at maxima. For abscissa the units are in m^3/mol for adsorption constants and J/mol for activation energies.

The estimated values of the rate constants and the activation energies altogether with the relative low standard errors are listed in Table 2 having the degree of explanation of 99.83 %. The

results presented in Figure 9 clearly demonstrate that the model is able to capture the experimentally observed molar fluxes for ethanol oxidative dehydrogenation in an excellent way.

Table 2. Parameter estimation results, where k'_i is the pre-exponential factor and E_a is the activation energy of the corresponding reactions

Parameter	Value	Units	Standard error, %
k'_{I} ***(eq. 13)***	$0.9*10^{-4}$	$m^3.g^{-1}.\ mol^{-1}min^{-1}$	3.8
k'_{II} ***(eq. 16)***	$3.3*10^{-2}$	$m^6.g^{-1}.\ mol^{-2}min^{-1}$	33
k'_{III} ***(eq. 17)***	$0.1*10^{-4}$	$m^3.g^{-1}.\ mol^{-1}min^{-1}$	17.7
$E_{a_{\text{I}}}$	75	*kJ/mol*	n.d
$E_{a_{\text{II}}}$	15	*kJ/mol*	n.d
$\boldsymbol{E_{a_{\text{III}}}}$	105	*kJ/mol*	n.d

n.d.- not determined as the values were fixed based on Monte Carlo Markov Chain analysis.

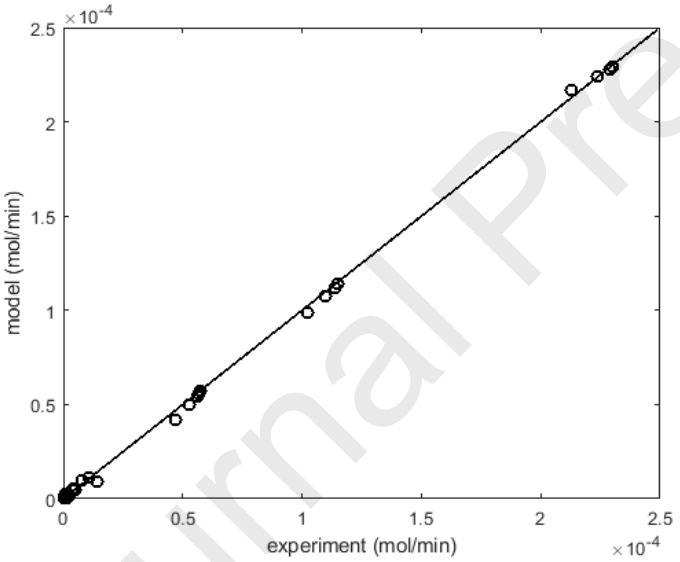

Figure 9. Comparison between the experimental values of molar fluxes of reactants (dots) and the calculations (lines).

3.3.5. Reaction and diffusion in the porous catalyst layer

The developed kinetic model agrees well with DFT computed values and can explain the experimental data. Experimental data generated in fixed bed reactors could in principle be influenced by external and internal mass transfer limitations. To confirm that the reaction was conducted in the kinetic regime and the regressed parameters correspond to the conditions of

intrinsic kinetics, the concentration profiles in the catalyst layers with different thicknesses were calculated.

A dynamic model for the reaction and internal diffusion was used to obtain the concentration profiles and get the insight in the dynamics of the porous catalyst layer. Because rather thin catalyst layers in the semi-elliptical channels are considered, the catalyst layer was regarded as a slab. Consequently, the mass balance for a component in the porous layer becomes:

$$\frac{\partial c_i}{\partial t} = \frac{1}{\varepsilon_p}(D_{ei}\frac{\partial c_i^2}{\partial r^2} + r_i\rho_p) \qquad (24)$$

where is c is concentration, t is the time, D_{ei} is the effective diffusion coefficient, while ε_p and ρ_p denote the particle porosity and density, and r_i is the component generation rate. The molecular diffusion coefficient were estimated from the Fuller-Schettler equation [69]. The numerical values of the diffusion coefficients calculated were updated inside the catalyst layer. The system of parabolic partial differential equations (PDE) (24) was discretized with central finite differences and the system of ordinary differential equations (ODEs) created was solved with respect to time using a stiff ODE solver based on backward differences. A more detailed discussion on the general methodology for numerical simulations of concentration profiles is presented in ref. [65]. The simulation results for the ethanol concentrations in the catalyst layers with 50-1500 μm thickness are shown in Figure 10.

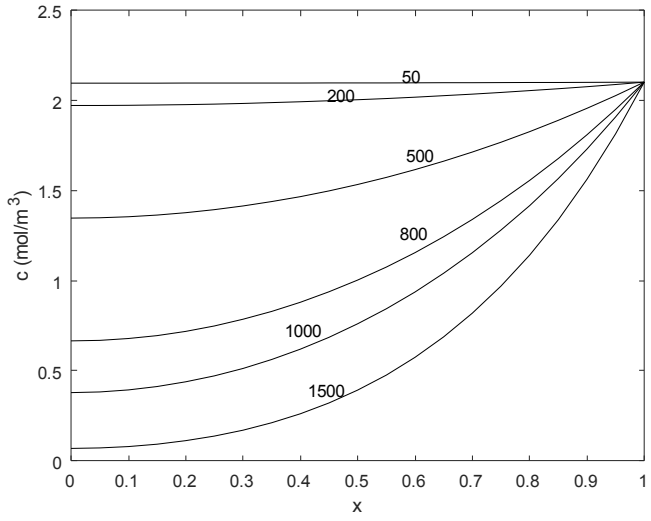

Figure 10. Concentration profile of ethanol at 250°C inside the catalyst layer with different thicknesses (number are given in μm). The length coordinate equals to unity at the surface of the catalyst layer and becomes zero at the bottom of the layer.

The simulations were done for the highest ethanol conversion *i.e.,* the highest residence time (0.07 s) and temperature (250°C). The results indicate that there are no internal mass transfer limitations for the layer thicknesses less than 200 μm. Since the experimental results in this work were carried out in a reactor having catalyst particles of the size ca. 30 μm the reaction was not influenced by the internal diffusion limitations in the catalyst pores.

As diffusion limitations might affect the activation energy of a reaction, the activation energy obtained in this work was compared with the literature data. The activation energy (75 kJ/mol) is considerably higher than the values reported in the literature for the ethanol oxidation on different supported gold catalysts. An apparent activation energy of 35 kJ/mol over Au/MCM-41 within the temperature range of 170-185°C was reported by Guan and Hensen [7]. The apparent activation energies for different CeO_2 supported gold catalysts were in the range of 22-50 kJ/mol [70]. A similar value of the apparent activation energy (49 kJ/mol) was observed over Au/SiO_2 catalyst at 120-180°C [71]. Although the average gold particle size (1.8 nm) was similar to the catalyst used in this study (~2 nm), the catalyst particle size was considerably larger (125-250 μm). The apparent activation energy for the oxidation of ethanol on Au/CeZr

cordierite monolithic catalysts with unspecified thickness at 50-300°C was 84 kJ/mol in [72] similar to that of the current work.

The difference in the activation energies might be correlated to the diffusion limitations in previous works. If a reaction is strongly influenced by diffusion, the effectiveness factor is proportional to the reciprocal value of the Thiele modulus $\eta_{e,i} = 1/\varphi_i$ where $\varphi_i = \sqrt{(kc_i^{n-1}/D_{e,i})}\, R_l$ [65] implying that r_i' is proportional to $\sqrt{k} = \sqrt{Ae^{-E_a/RT}}$. The apparent activation energy is $\frac{1}{2}E_a$ in the extreme case, which might explain the differences between the values of the activation energy in this work and the literature. However, it should be kept in mind that the apparent activation energy depends on the details of the kinetic models and can deviate significantly from the true activation energy [73]. Moreover, the activation energies should be compared at the same reactant concentrations and in the general case could depend on the metal cluster size [74].

4. Conclusions

In the present work experimental and computational studies were performed to understand the mechanism of oxidative dehydrogenation of ethanol over gold on alumina. The catalysts with the metal loading of ca. 1 wt% and the particle size ranging from ca. 2 to 7 nm were prepared by the deposition- precipitation method and studied in a laboratory scale fixed bed reactor operating at temperatures 130 - 250^{o}C and atmospheric pressure. The critical role of oxygen in the oxidative dehydrogenation was also demonstrated by low activity towards acetaldehyde and preferential dehydration to ethylene on acid sites of the catalyst support in the absence of O_2. In the presence of oxygen, acetaldehyde was the main product.

Computational studies on the catalytic pathways were performed accounting for the van der Waals dispersion effects. The theoretical analysis revealed the key features of the reaction mechanism: molecular adsorption of dioxygen, oxygen assisted dissociative adsorption of ethanol with the formation of ethoxy and peroxy species, decomposition of the latter to O and OH species, recombination of hydroxyls giving water and adsorbed oxygen. The latter either reacts with ethoxy species with the formation of acetaldehyde or recombines to dioxygen. The computational studies show that activation of molecular oxygen does not proceed on a bare gold surface. However, the presence of a hydrogen bond donor e.g., ethanol, facilitates O-O bond rupture through formation of an OOH intermediate by abstraction of a proton from the bond donor. In the reaction pathway from oxygen and ethanol to the main reaction products acetaldehyde and water, the main intermediates are peroxy (OOH), ethoxy species as well as O and OH formed from the peroxy intermediate.

Based on the DFT considerations a kinetic model was developed. The model was supplemented with kinetic equations accounting for the formation of diethyl ether and ethyl acetate. Numerical data fitting demonstrated an adequate description of the representative experimental data with statistically well-identified parameters. The value of the activation energy computed by DFT

for the rate-limiting step of O_2 hydrogenation to OOH where EtOH is the hydrogen donor was directly used in numerical data fitting. This rate-limiting step is followed by the irreversible acetaldehyde formation step which makes the overall reaction thermodynamically favorable. It was also shown that the current kinetic experiments are free from mass transfer effects and that the obtained kinetic parameters reflect the true kinetics of the reaction. Performed simulations revealed that the role of mass transfer becomes prominent for catalyst particles exceeding 200 μm, while in the current experimental work the catalyst particles were 20-30 μm.

In conclusion, experimental and computational work performed in this study allowed to propose a feasible mechanism that was able to adequately describe experimental data. In the proposed mechanism the oxidative dehydrogenation of ethanol over an alumina-supported gold catalyst is assisted by synergetic interactions between molecular oxygen and ethanol. The latter reactant provides hydrogen bonding needed to dissociate molecular O_2 giving reactive oxygen species required in oxidative dehydrogenation of ethanol to acetaldehyde. Besides detailed understanding of the reaction mechanism, a DFT-inspired kinetic model successfully explained both experimental and computational results forming a solid basis towards developing selective alcohol dehydrogenation catalysts.

Acknowledgements

This work is a part of the activities of Johan Gadolin Process Chemistry Centre (PCC) at Åbo Akademi University. EB acknowledges Graduate School in Chemical Engineering (GSCE) for a PhD grant. TS acknowledges the Academy Professor grant (project 319002) from Academy of Finland. MMM acknowledges support from the Alfred Kordelin foundation and the Academy of Finland for the post-doctoral grant (project 307853). The computer resources were provided by CSC - IT Center for Science Ltd.

Author Contributions

EB and MMM contributed equally. EB conducted the experimental work and MMM was responsible for the computational studies. All authors contributed to the kinetic simulations and writing of the manuscript.

References

[1] R. Sheldon, I.W.C.E. Arends, G-J. Ten Brink, A. Dijksman, Green, catalytic oxidations of alcohols, Acc. Chem. Res. 35 (2002) 774–781.

[2] R. A. Sheldon, Recent advances in green catalytic oxidations of alcohols in aqueous media, Catal Today, 247 (2014) 4–13.

[3] X. Yao, C. Bai, J. Chen, Y. Li, Efficient and selective green oxidation of alcohols by MOF-derived magnetic nanoparticles as a recoverable catalyst, RSC Adv. 6 (2016) 26921–26928.

[4] J. C. Escobar, E.S. Lora, O.J. Venturini, E.E. Yanez, C.E.F, O. Almazan, Biofuels: Environment, technology and food security, Renewable Sustainable Energy Rev. 13 (2009) 1275–1287.

[5] C.H. Christensen, B. Jørgensen, J. Rass-Hansen, K. Egeblad, R. Madsen, S.K. Klitgaard, S.M. Hansen, M.R. Hansen, H.C. Andersen, A. Riisager, Formation of acetic acid by aqueous-phase oxidation of ethanol with air in the presence of a heterogeneous gold catalyst, Angew. Chem. Int. Edit. 45 (2006) 4648–4651.

[6] Global energy transformation: A roadmap to 2050, International Renewable Energy Agency (IRENA), Abu Dhabi, 2018

[7] Y. Guan, E. M. Hensen, Ethanol dehydrogenation by gold catalysts: The effect of the gold particle size and the presence of oxygen, Appl. Catal. A: Gen. 361 (2009) 49-56.

[8] M. Boronat, A. Corma, F. Illas, J. Radilla, T. Ródenas, M. J. Sabater, Mechanism of selective alcohol oxidation to aldehydes on gold catalysts: Influence of surface roughness on reactivity, J. Catal. 278 (2011) 50-58.

[9] H. Liu, Y. Liu, Y. Li, Z. Tang, H. Jiang, Metal− organic framework supported gold nanoparticles as a highly active heterogeneous catalyst for aerobic oxidation of alcohols, J. Phys. Chem. C, 114 (2010) 13362–13369.

[10] A. Quintanilla, V. Butselaar-Orthlieb, C. Kwakernaak, W. Sloof, M. Kreutzer, F. Kapteijn, Weakly bound capping agents on gold nanoparticles in catalysis: Surface poison?, J. Catal. 271 (2010) 104–114.

[11] Y. Zhang, X. Cui, F. Shi, Y. Deng, Nano-gold catalysis in fine chemical synthesis, Chem. Rev. 112 (2012) 2467–2505.

[12] R. Ciriminna, E. Falletta, C. Della Pina, J.H. Teles, M. Pagliaro, Industrial applications of gold catalysis, Angew. Chem. Int. Edit. 55 (2016) 14210–14217.

[13] A. Lackmann, C. Mahr, M. Schowalter, L. Fitzek, J. Weissmüller, A. Rosenauer, A. Wittstock, A comparative study of alcohol oxidation over nanoporous gold in gas and liquid phase, J. Catal. 353 (2017) 99–106.

[14] S. Meenakshisundaram, E. Nowicka, P.J. Miedziak, G.L. Brett, R.L. Jenkins, N. Dimitratos, S.H. Taylor, D.W. Knight, D. Bethell, G.J. Hutchings, Oxidation of alcohols using supported gold and gold–palladium nanoparticles, Faraday Discuss. 145 (2010) 341–356.

[15] A. Abad, A. Corma, H. García, Catalyst parameters determining activity and selectivity of supported gold nanoparticles for the aerobic oxidation of alcohols: The molecular reaction

mechanism, Chem.-A Eur. J. 14 (2008) 212–222.

[16] J. Sun, X. Tong, Z. Liu, S. Liao, S. Xue, Gold-catalyzed selectivity-switchable oxidation of benzyl alcohol in the presence of molecular oxygen, Catal. Comm. 85 (2016) 70–74.

[17] E. Behravesh, N. Kumar, Q. Balme, J. Roine, J. Salonen, A. Schukarev, J.-P. Mikkola, M. Peurla, A. Aho, K. Eränen, D.Yu. Murzin, T. Salmi, Synthesis and characterization of Au nano particles supported catalysts for partial oxidation of ethanol: Influence of solution pH, Au nanoparticle size, support structure and acidity, J. Catal. 353 (2017) 223–238.

[18] M. Alhumaimess, Z. Lin, W. Weng, N. Dimitratos, N.F. Dummer, S.H. Taylor, J.K. Bartley, C.J. Kiely, G.J. Hutchings, Oxidation of benzyl alcohol by using gold nanoparticles supported on ceria foam, CHEMSUSCHEM, 5 (2012) 125–131.

[19] S.K. Klitgaard, A.T. DeLa Riva, S. Helveg, R.M. Werchmeister, C.H. Christensen, Aerobic oxidation of alcohols over gold catalysts: Role of acid and base, Catal. Lett. 126 (2008) 213–217.

[20] M.L. Personick, R.J. Madix, C.M. Friend, Selective oxygen-assisted reactions of alcohols and amines catalyzed by metallic gold: Paradigms for the design of catalytic processes, ACS Catal. 7 (2017) 965–985.

[21] K. Sakata, K. Tada, S. Yamada, Y. Kitagawa, T. Kawakami, S. Yamanaka, M. Okumura, DFT calculations for aerobic oxidation of alcohols over neutral Au_6 cluster, Mol. Phys. 112 (2014) 385–392.

[22] C. Shang and Z.-P. Liu, Origin and activity of gold nanoparticles as aerobic oxidation catalysts in aqueous solution, J. Am. Chem. Soc. 133 (2011) 9938–9947.

[23] A. Abad, P. Concepción, A. Corma, H. García, A collaborative effect between gold and a support induces the selective oxidation of alcohols, Angew. Chem. Int. Edit. 44 (2005) 4066–4069.

[24] S. Hong and T.S.R. Rahman, Rationale for the higher reactivity of interfacial sites in methanol decomposition on $Au_{13}/TiO_2(110)$, J. Am. Chem. Soc. 135 (2013) 7629–7635.

[25] M. Farnesi Camellone, J. Zhao, L. Jin, Y. Wang, M. Muhler, D. Marx, Molecular understanding of reactivity and selectivity for methanol oxidation at the Au/TiO_2 interface, Angew. Chem. Int. Edit, 52 (2013) 5780–5784.

[26] B. Hvolbaek, T. V.W. Janssens, B. S. Clausen, H. Falsig, C.H. Christensen, J.K. Norskov, Catalytic activity of Au nanoparticles, Nanotoday 2 (2007) 14-18.

[27] J. Kim, E. Samano, B.E. Koel, Oxygen adsorption and oxidation reactions on Au (211) surfaces: Exposures using O_2 at high pressures and ozone (O_3) in UHV, Surf. Sci. 600 (2006) 4622-4632.

[28] Y. Xu, M. Mavrikakis, Adsorption and dissociation of O_2 on gold surfaces: Effect of steps and strain, J. Phys. Chem. B, 107 (2003) 9298–9307

[29] G. Tomaschun, W. Dononelli, Y.Li, M. Bäumer, T. Klüner, L.V. Moskaleva, Methanol oxidation on the Au (310) surface: A theoretical study, Journal of Catalysis 364 (2018) 216–227

[30] A. Roldán, S. González, J.M. Ricart, F. Illas, Critical size for O_2 dissociation by Au nanoparticles, CHEMPHYSCHEM, 10 (2009) 348–351.

[31] M. Boronat, A. Corma, Molecular approaches to catalysis: Naked gold nanoparticles as quasi-molecular catalysts for green processes, J. Catal. 284 (2011) 138–147.

[32] B. Xu, J. Haubrich, T. Baker, E. Kaxiras, C. M. Friend, Theoretical study of O-assisted selective coupling of methanol on Au(111), J. Phys. Chem. C, 115 (2011) 3703–3708.

[33] M. Qingsen, S. Yongli, X. Jing, G. Jinlong, Mechanistic insights into selective oxidation of ethanol on Au(111): A DFT study, Chin. J. Catal. 33 (2012) 407–415.

[34] J. Gong, D.W. Flaherty, R.A. Ojifinni, J.M. White, C.B. Mullins, Surface chemistry of methanol on clean and atomic oxygen pre-covered Au(111), J. Phys. Chem. C, 112 (2008) 5501–5509.

[35] J. Gong, D.W. Flaherty, T. Yan and C.B. Mullins, Selective oxidation of propanol on Au(111): Mechanistic insights into aerobic oxidation of alcohols, ChemPhysChem, 9 (2008) 2461–2466.

[36] T. Yan, J. Gong, C.B. Mullins, Oxygen exchange in the selective oxidation of 2-butanol on oxygen precovered Au(111), J. Am. Chem. Soc. 131 (2009) 16189–16194.

[37] J. Gong, C.B. Mullins, Selective oxidation of ethanol to acetaldehyde on gold, J. Am. Chem. Soc. 130 (2008) 16458–16459.

[38] X. Liu, B. Xu, J. Haubrich, R.J. Madix, C. M. Friend, Surface-mediated self-coupling of ethanol on gold, J. Am. Chem. Soc. 131 (2009) 5757–5759.

[39] C.R. Chang, Z.Q. Huang, J. Li, Hydrogenation of molecular oxygen to hydroperoxyl: An alternative pathway for O_2 activation on nanogold catalysts, Nano Res. 8 (2015) 3737–3748.

[40] C.R. Chang, X.F. Yang, B. Long, J. Li, A water-promoted mechanism of alcohol oxidation on a Au(111) surface: Understanding the catalytic behavior of bulk gold, ACS Catal. 3 (2013) 1693–1699.

[41] D. Muñoz-Santiburcio, D. Farnesi Camellone, D. Marx, Solvation-induced changes in the mechanism of alcohol oxidation at gold/titania nanocatalysts in the aqueous phase versus gas phase, Angew. Chem. Int. Edit, 57 (2018) 3327–3331.

[42] G.M. Mullen, E.J. Evans, I. Sabzevari, B.E. Long, K. Alhazmi, B.D. Chandler, C. B. Mullins, Water influences the activity and selectivity of ceria-supported gold catalysts for oxidative dehydrogenation and esterification of ethanol, ACS Catal. 7 (2017) 1216–1226.

[43] H.V. Tran, H.A. Doan, B.D. Chandler, L.C. Grabow, Water-assisted oxygen activation during selective oxidation reactions, Curr. Opin. Chem. Eng. 13 (2016) 100–108.

[44] J.R. Anderson, Structure of metallic catalysts, London: Academic Press, 1975.

[45] D.Yu. Murzin, Engineering catalysis, Belrin: De Gryuter, 2020.

[46] J.J. Mortensen, L.B. Hansen, K.W. Jacobsen, Real-space grid implementation of the projector augmented wave method, Phys. Rev. B. 71 (2005) 035109.

[47] P.E. Blöchl, Projector augmented wave method, Phys. Rev. B 50 (1994) 17953.

[48] J. Wellendorff, K.T. Lundgaard, A. Møgelhøj, V. Petzold, D.D. Landis, J.K. Nørskov, T. Bligaard, K. W. Jacobsen, Density functionals for surface science: Exchange-correlation model development with Bayesian error estimation, Phys. Rev. B, 85 (2012) 235149–235171.

[49] E. Bitzek, P. Koskinen, F. Gähler, M. Moseler, P. Gumbsch, Structural relaxation made simple, Phys. Rev. Lett, 97 (2006) 170201-1–170201-4.

[50] G. Henkelman, H. Jónsson, Improved tangent estimate in the nudged elastic band method for finding minimum energy paths and saddle points, J. Chem. Phys. 113 (2000) 9978–9985.

[51] G. Henkelman, B.P. Uberuaga, H. Jonsson, A climbing image nudged elastic band method for finding saddle points and minimum energy paths, J. Chem. Phys. 113 (2000) 9901–9904.

[52] A.H. Larsen, J.J. Mortensen, J. Blomqvist, I.E. Castelli, R. Christensen, M. Dułak, J. Friis, M.N. Groves, B. Hammer, C. Hargus, E.D. Hermes, P.C. Jennings, P.B. Jensen, J. Kermode, J.R. Kitchin, E.L. Kolsbjerg, J. Kubal, K. Kaasbjerg, et. al. The atomic simulation environment-a Python library for working with atoms, J. Phys. Cond. Matt. 29 (2017) 273002–273031.

[53] S. Smidstrup, A. Pedersen, K. Stokbro, H. Jónsson, Improved initial guess for minimum energy path calculations, J. Chem. Phys. 140 (2014) 214106–214119.

[54] T.A. Baiker, C.M. Friend, E.Kaxiras, Atomic oxygen adsorption on Au(111) surfaces with defects, J. Phys. Chem. C., 113 (2009) 3232-3238.

[55] A.J.R. Hensley, K. Ghale, C. Rieg, T. Dang, E. Anderst, F. Studt, C.T. Campbell, J.-S. McEwen, Y. Xu, DFT-based method for more accurate adsorption energies: An adaptive sum of energies from RPBE and vdW density functionals, J. Phys. Chem. 121 (2017) 4937–4945.

[56] A.Roldan, G. Gonzales, J.M. Ricart and F. Illas, Critical size for O2 dissociation by gold nanoparticles, ChemPhysChem 10, (2009) 348-351.

[57] J. K. Nørskov, T. Bligaard, A. Logadottir, S. Bahn, L. B. Hansen, M. Bollinger, H. Bengaard, B. Hammer, Z. Sljivancanin, M. Mavrikakis, Y. Xu, S. Dahl, and C. J. H. Jacobsen, Universality in heterogeneous catalysis , J. Catal. 209 (2002), 275-278 .

[58] R.L.H. Freire, D. Guedes-Sobrinho, A. Kiejna, J.L.F. Da Silva, Comparison of the performance of van der Waals dispersion functionals in the description of water and ethanol on transition metal surfaces, J. Phys. Chem. 122 (2018) 1577–1588.

[59] B. Xu, R.J. Madix, C.M. Friend, Achieving optimum selectivity in oxygen assisted alcohol cross-coupling on gold, J. Am. Chem. Soc. 132 (2010) 16571-16580.

[60] Z.-P. Liu, P. Hu, A. Alavi, Catalytic role of gold in gold-based catalysts: A Density Functional Theory study on the CO oxidation on gold, J. Am. Chem. Soc. 124 (2002), 1477-14770

[61] X. Deng, B.K. Min, A. Guloy, C.M. Friend, Enhancement of O_2 dissociation on Au(111) by adsorbed oxygen: Implications for oxidation catalysis, J. Am. Chem. Soc. 127 (2005) 9267–9270.

[62] E. Behravesh, K. Eränen, N. Kumar, J. Peltonen, M. Peurla, A. Aho, M. Nurmi, M. Toivakka, D. Murzin, T. Salmi, Microreactor coating with Au/Al_2O_3 catalyst for gas-phase partial oxidation of ethanol: Physico-chemical characterization and evaluation of catalytic properties, Chem. Eng. J. In Press, 2019.

[63] M.I. Temkin, The kinetics of some industrial heterogeneous catalytic reactions, Adv. Catal. 28 (1079) 173–291.

[64] H. Haario, Modest 6.0-A User's Guide, ProfMath, Helsinki, 2001.

[65] D. Murzin, T. Salmi, Catalytic Kinetics, 2nd ed., Amsterdam: Elsevier, 2016.

[66] L. Görlitz, Z. Gao, W. Schmitt, Statistical analysis of chemical transformation kinetics using Markov-Chain Monte Carlo methods, Environ. Sci. Technol. 45 (2011) 4429-4437.

[67] H. Haario, E. Saksman, J. Tamminen, An adaptive Metropolis algorithm, Bernoulli, 7 (2001) 223–242.

[68] S. Matera, W. F. Schneider, A. Heyden, A. Savara, Progress in accurate chemical kinetic modeling, simulations, and parameter estimation for heterogeneous catalysis, ACS Catal. 9 (2019) 6624-6647.

[69] E.N. Fuller, P.D. Schettler, J.C. Giddings, New method for prediction of binary diffusion coefficients, Ind. Eng. Chem. 58 (1966) 18-27.

[70] G.M. Mullen, E.J. Evans JR, B.C. Siegert, N.R. Miller, B.K. Rosselet, I. Sabzevari, A. Brush, Z. Duan C.B. Mullins, The interplay between ceria particle size, reducibility, and ethanol oxidation activity of ceria-supported gold catalysts, React. Chem. Eng. 3 (2018) 75–85.

[71] Y. Guan, E.J.M. Hensen, Selective oxidation of ethanol to acetaldehyde by Au−Ir catalysts, J. Catal. 305 (2013) 135–145.

[72] P. Topka, M. Klementová, Total oxidation of ethanol over Au/$Ce_{0.5}Zr_{0.5}O_2$ cordierite monolithic catalysts, Appl. Catal. A: Gen. 522 (2016) 130–137.

[73] G. Bond, M. Keane, H. Kral, J. Lercher, Compensation phenomena in heterogeneous catalysis: General principles and a possible explanation, Catal. Rev. 42 (2000) 323–383.

[74] D. Murzin, On apparent activation energy of structure sensitive heterogeneous catalytic reactions, Catal. Lett. 149 (2019) 1455–1463.

Graphical abstract for TOC only

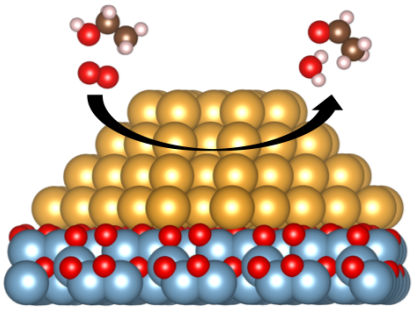

Highlights

- Ethanol oxidative dehydrogenation to acetaldehyde on gold catalysts
- Catalytic experiments, density functional theory (DFT) and kinetic modelling
- Activation of molecular oxygen is aided by the hydrogen bond donor
- Adequate description of kinetic data based on the DFT derived mechanism
- Evaluation of the role of diffusion in the catalyst pores.